

Limitation enhancement of a mixed convection by a vibrational heat surface in a vertical channel

Wu-Shung Fu · Chien-Ping Huang

Received: 18 December 2006 / Accepted: 2 May 2007 / Published online: 20 June 2007
© Springer-Verlag 2007

Abstract A numerical simulation is performed to study effects of a vibrational heat surface on a mixed convection in a vertical channel flow. This subject is a kind of moving boundary problems, and the finite element method and arbitrary Lagrangian–Eulerian kinematics description method is then utilized. The main parameters of Grashof number, amplitude and frequency are taken into consideration, and the Reynolds number is limited and equals 100. According to the results, the equations of the critical vibration frequency could be derived and expressed in terms of Grashof number and amplitude. In the forced convection, the critical vibration frequency is only dependent on the amplitude, and in the mixed convection the critical vibration frequency becomes larger as the Grashof number increases. The variation of the critical vibration frequency of the study could league with the critical vibration frequency of the natural convection shown in the previous study consistently.

List of symbols

f_c	vibration frequency of heat surface (1/s)
F_c	dimensionless vibration frequency of heat surface
F_{cc}	dimensionless critical vibration frequency
g	acceleration of gravity (m/s ²)
Gr	Grashof number
ℓ_0	length of channel (m)
ℓ_1	length from heat surface to top (m)
ℓ_2	length of heat surface (m)
ℓ_3	length from heat surface to bottom (m)
ℓ_c	vibration amplitude of heat surface (m)
L_2	dimensionless length of heat surface
L_3	dimensionless length from heat surface to bottom
L_c	dimensionless vibration amplitude of heat surface
Nu_Y	local Nusselt number
Nu	average Nusselt number
\overline{Nu}	time-average Nusselt number
Nu_{st}	average Nusselt number at the stationary state
p	pressure (N/m ²)
P	dimensionless pressure
Pr	Prandtl number
Ra	Rayleigh number
Re	Reynolds number
t	time (s)
T	temperature (K)
T_c	ambient temperature (K)
T_h	temperature of heat surface (K)
u, v	velocities in x and y directions (m/s)
U, V	dimensionless velocities in x and y directions
u_c	vibration velocity of heat surface (m/s)
U_c	dimensionless vibration velocity of heat surface
u_m	maximum vibration velocity of heat surface (m/s)
U_m	dimensionless maximum vibration velocity of heat surface
\hat{u}	mesh velocity in x direction (m/s)

W.-S. Fu (✉)

Department of Mechanical Engineering,
National Chiao Tung University,
1001 Ta Hsueh Road, Hsinchu 30056,
Taiwan, ROC
e-mail: wsfu@mail.nctu.edu.tw

C.-P. Huang

Department of Mechanical Engineering,
National Chiao Tung University
(Energy and Environment Research Laboratories,
Industrial Technology Research Institute),
Hsinchu, Taiwan, ROC

\hat{U}	dimensionless mesh velocity in x direction
w	width of channel (m)
x, y	Cartesian coordinates (m)
X, Y	dimensionless Cartesian coordinates

Greek symbols

α	thermal diffusivity (m^2/s)
β	volume coefficient of expansion (1/K)
θ	dimensionless temperature
λ	penalty parameter
ν	kinematic viscosity (m^2/s)
ρ	density (kg/m^3)
τ	dimensionless time
τ_P	dimensionless period time

1 Introduction

In a practical case, devices in a system are always under dynamic situation due to the operation of the system, which results in the devices being unavoidably subject to a vibrational motion. To validate the effect of the vibration motion on the structure or heat transfer rate of the devices then becomes an urgent need for the design of precise and effective device.

Effects of a vibrational motion on natural convection heat transfer of a heated surface in a vertical channel were investigated by Fu and Huang [2] in detail and the relating literature were also reviewed. Numerous dynamic phenomena were first revealed and an important factor of critical vibration frequency F_{cc} was proposed. As the frequency of the vibrational motion of the heat surface was larger than the critical vibration frequency F_{cc} , the natural convection heat transfer of the heat surface could be enhanced and vice versa. This result is opposite to the existing concept of the vibrational motion unconditionally enhancing the heat transfer of the heat surface. However, to the knowledge of the authors without literature validates the phenomena mentioned above could infer to those of a mixed flow.

A mixed flow effected by a vibrational motion belongs to a kind of moving boundary problems. Similar objects were investigated in the past. Kang and Jaluria [6, 7] had studied the mixed convection flow in a channel subject to a continuously moving material. The aim of those studies was to find the better cooling rate of the forming manufacturing processes. Meric [8] studied an optimization of shape and flow parameters for combined free and forced convection flows through vertical rectangular channels with moving walls. Optimal values of these design

parameters had been determined in order to obtain a uniform distribution of the axial velocity within the channel with a fixed flow rate. The results indicated that the optimal values of the wall velocity and the axial pressure gradient increased with the increment of Rayleigh number in the meantime the optimal value of the channel height decreased. Andreozzi et al. [1] also used a numerical method to analyze an opposing mixed convection of air in a vertical channel with a moving plate. The results showed that as the velocity of the moving plate increased the maximum wall temperature decreased because of the formation of a reversed forced flow in the channel. As for a problem of effects of a vibrational heat surface on a mixed flow in a channel is seldom investigated.

The aim of this study is therefore to study a mixed convection affected by a vibrational heat surface in a vertical channel. Due to the interaction between the fluid and the heat surface, the flow and thermal fields become time-dependent and belong to a kind of moving boundary problem. It is hardly analyzed by either the Lagrangian or the Eulerian kinematic description methods solely for simulating the problem more realistically, an arbitrary Lagrangian–Eulerian (ALE) kinematic description method by Hirt et al. [4], is then adopted to describe the problem. It combines the characteristics of the Lagrangian and Eulerian kinematic description method, and is an appropriate kinematic description method.

The effects of the Grashof number, vibration frequency and amplitude of the heat surface on the mixed flow structures and heat transfer characteristics are investigated. The critical vibration frequency F_{cc} for the mixed flow is obtained and the relating correlation equations which could connect smoothly with the relating correlation equations of the natural convection obtained by Fu and Huang [2] are derived.

2 Physical model

A physical model used in this study is shown in Fig. 1. A two-dimensional vertical channel with length and width are ℓ_0 and w , respectively. The vibrational heat surface with length ℓ_2 is on the left sidewall. The length ℓ_1 is from the top of the heat surface to the top of the channel and the length ℓ_3 is from the bottom of the heat surface to the bottom of the channel. The temperature of vibrational heat surface is constant and equals to T_h which is higher than the inlet temperature T_c of the fluid. The walls are insulated except the heat surface. The inlet velocity of the fluid is v_0 . As the time $t > 0$, the heat surface is subject to a vibrational motion, which is normal to the gravity direction with the frequency f_c and amplitude ℓ_c . The variations of the flow

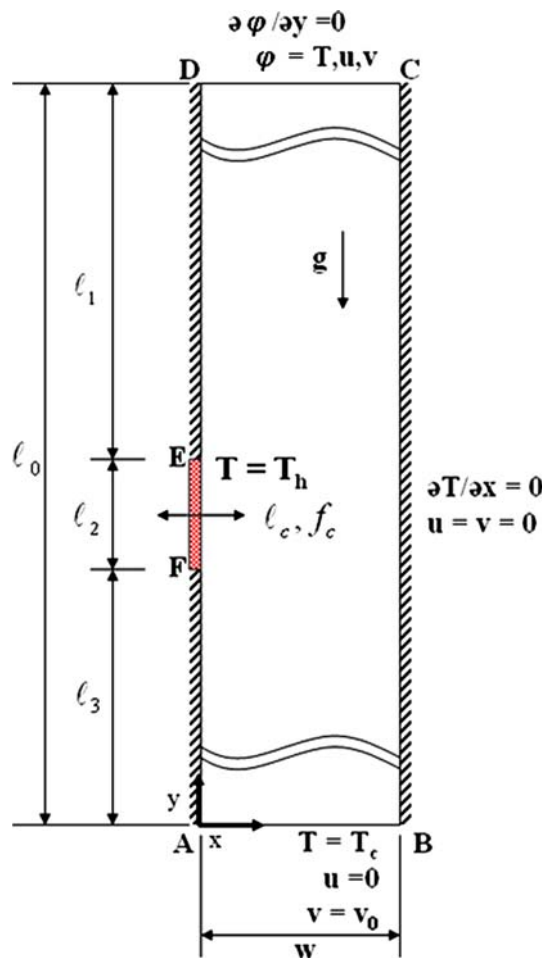


Fig. 1 Physical model

field affected by the vibrational heat surface become time dependent and are classified into a class of moving boundary problems. As a result, the ALE method is properly utilized to analyze this subject.

The main heat transfer mechanism in this study is based on the interaction between the vibration motion of the heat surface and the flowing fluid. The direction of vibration motion of the heat surface is vertical to the channel, and the left wall containing the heat surface becomes convex and concave alternatively. As the heat surface is convex, the heated fluid is easily departed from the heat surface, which is beneficial to the heat transfer rate. Oppositely, the concave heat surface is disadvantageous to the heat transfer rate due to the stagnation of the heated fluid in the concavity and the heated fluid is difficult to depart from the heat surface; unless that the frequency and amplitude of vibration motion are quick and large enough to conquer the barrier of the concave situation.

For facilitating the analysis, the following assumptions are made.

1. The flow field is two-dimensional and laminar.
2. The fluid is air, Newtonian and incompressible.
3. The fluid properties are constant except density.
4. The non-slip condition is held on the interfaces between the fluid and heat surface.

Based upon the characteristics scales of ℓ_2 , T_h , T_c and v_0 , the dimensionless variables and governing equation are defined as follows:

$$\begin{aligned} X &= \frac{x}{\ell_2}, \quad Y = \frac{y}{\ell_2}, \quad \tau = \frac{tv_0}{\ell_2}, \quad U = \frac{u}{v_0}, \quad V = \frac{v}{v_0}, \\ \hat{U} &= \frac{\hat{u}}{v_0}, \quad P = \frac{P}{\rho_0 v_0^2}, \quad Re = \frac{\rho_0 v_0 \ell_2}{\mu} = \frac{v_0 \ell_2}{\nu}, \\ F_c &= \frac{f_c \ell_2}{v_0} L_c = \frac{\ell_c}{\ell_2}, \quad \theta = \frac{T - T_c}{T_h - T_c}, \\ \text{Pr} &= \frac{\nu}{\alpha}, \quad Gr = \frac{g \beta (T_h - T_c) \ell_2^3}{\nu^2} \end{aligned} \quad (1)$$

where \hat{u} is the mesh velocity, ℓ_c and f_c are the vibrational amplitude and frequency, respectively.

Continuity equation

$$\frac{\partial U}{\partial X} + \frac{\partial V}{\partial Y} = 0 \quad (2)$$

Momentum equations

$$\frac{\partial U}{\partial \tau} + (U - \hat{U}) \frac{\partial U}{\partial X} + V \frac{\partial U}{\partial Y} = - \frac{\partial P}{\partial X} + \frac{1}{Re} \left(\frac{\partial^2 U}{\partial X^2} + \frac{\partial^2 U}{\partial Y^2} \right) \quad (3)$$

$$\begin{aligned} \frac{\partial V}{\partial \tau} + (U - \hat{U}) \frac{\partial V}{\partial X} + V \frac{\partial V}{\partial Y} &= - \frac{\partial P}{\partial Y} \\ &+ \frac{1}{Re} \left(\frac{\partial^2 V}{\partial X^2} + \frac{\partial^2 V}{\partial Y^2} \right) + \frac{Gr}{Re^2} \theta \end{aligned} \quad (4)$$

Energy equations

$$\frac{\partial \theta}{\partial \tau} + (U - \hat{U}) \frac{\partial \theta}{\partial X} + V \frac{\partial \theta}{\partial Y} = \frac{1}{Pr Re} \left(\frac{\partial^2 \theta}{\partial X^2} + \frac{\partial^2 \theta}{\partial Y^2} \right) \quad (5)$$

The dimensionless vibration velocity U_c is calculated from the following equation.

$$U_c = U_m \cos(2\pi F_c \tau) \quad (6)$$

And the dimensionless maximum vibration velocity U_m can be obtained from the following equation.

$$U_m = 2\pi F_c L_c \quad (7)$$

As the time $\tau > 0$, the boundary conditions are as follows:

On the bottom side AB

$$U = 0, \quad V = 1, \quad \theta = 0 \quad (8)$$

Except the EF surface, the other surfaces of the channel are

$$U = 0, \quad V = 0, \quad \frac{\partial \theta}{\partial X} = 0 \quad (9)$$

On the top side CD

$$\frac{\partial U}{\partial Y} = 0, \quad \frac{\partial V}{\partial Y} = 0, \quad \frac{\partial \theta}{\partial Y} = 0 \quad (10)$$

On the EF surface

$$U = U_c, \quad V = 0, \quad \theta = 1 \quad (11)$$

3 Numerical method

The governing equations and boundary conditions are solved through the Galerkin finite element formulation and a backward scheme is adopted to deal with the time terms of the governing equations. The pressure is eliminated from the governing equations using the consistent penalty method. The velocity and temperature terms are expressed as quadrilateral element and eight node quadratic Lagrangian interpolation function. The Newton–Raphson iteration algorithm is utilized to simplify the nonlinear terms in the momentum equations. The discretization processes of the governing equations are similar to the one used in Fu and Yang [3].

A brief outline of the solution procedures are described as follows:

1. Determine the optimal mesh distribution and number of the elements and nodes.
2. Solve the values of the U , V and θ at the steady state and regard them as the initial conditions of the transient state.
3. Determine the time step $\Delta \tau$ and the mesh velocity \hat{u} of the computational meshes.
4. Update the coordinates of the nodes and examine the determinant of the Jacobian transformation matrix to ensure the one to one mapping to be satisfied during the Gaussian quadrature numerical integration.
5. Solve them until the following criteria for convergence are satisfied:

$$\left| \frac{\Phi^{m+1} - \Phi^m}{\Phi^{m+1}} \right|_{\tau + \Delta\tau} < 10^{-3}, \quad \text{where } \Phi = U, V \text{ and } \theta \quad (12)$$

6. Continue the next time step calculation until periodic solutions are attained.

4 Results and discussion

The working fluid is air with $Pr = 0.71$. The main parameters of Grashof number Gr , vibration amplitude L_c , and vibration frequency F_c are considered.

The local Nusselt number on the heat surface is calculated by the following equation.

$$Nu_Y = - \left. \frac{\partial \theta}{\partial X} \right|_{\overline{EF}} \quad (13)$$

The average Nusselt number on the heat surface is expressed as follows.

$$Nu = \frac{1}{L_2} \int_{L_3}^{L_3+L_2} Nu_Y dY \quad (14)$$

The time-averaged Nusselt number on the heat surface for per cycle is defined by

$$\overline{Nu} = - \frac{1}{\tau_p} \int_0^{\tau_p} Nu d\tau \quad (15)$$

In which τ_p is a periodical time and equals $1/F_c$.

For matching the boundary conditions at the top and bottom of the vertical channel mentioned above, the lengths from the top and bottom to the heat surface are determined by numerical tests and are equal to 81 and 21, respectively. To obtain an optimal computational mesh, four different non-uniform distributed elements are used for the mesh tests. Figure 2 shows the velocity and temperature profiles along the line through the center of the heat surface and parallel the X -axis at the steady state under $Gr = 10^4$ and $Re = 10^2$. Based upon the results, the computational mesh with 3,840 elements, which are corresponding to 12,185 nodes, are used for all cases in this study.

In addition, an implicit scheme is employed to deal with the time differential terms of the governing equations. Five different time steps $\Delta \tau = 5.0 \times 10^{-2}$, 2.5×10^{-2} , 1.25×10^{-2} , 5.0×10^{-3} , and 2.5×10^{-3} at $Gr = 10^4$, $Re = 10^2$, $L_c = 0.1$, and $F_c = 2$, are executed. The variations of the average Nusselt number on the heat surface Nu with time are shown in Fig. 3, and the time step $\Delta \tau = 1.25 \times 10^{-2}$ is chosen for this case. But the selected time step is different for each case of different Gr and L_c in this study.

The number of the time step of each period (period steps) is based on the results of time step test shown in Fig. 3 and is about 40. The frequency F_c is different for each case, and the dimensionless time step $\Delta \tau$ can be calculated from the following equation.

Fig. 2 Comparison of the velocity and temperature profiles along the line through the center of the heat surface and parallel the X -axis for different mesh ($Gr = 10^4$, $Re = 10^2$)

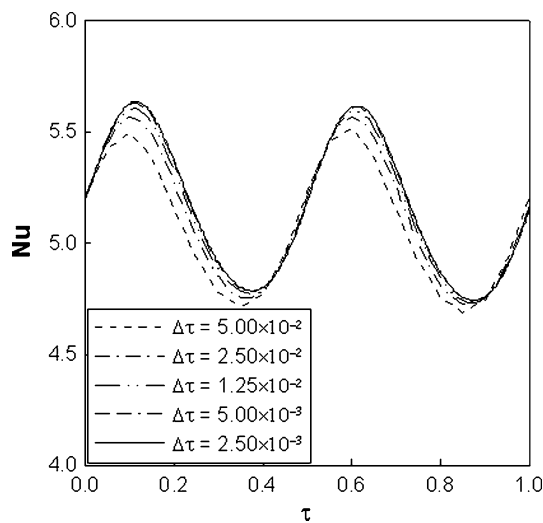
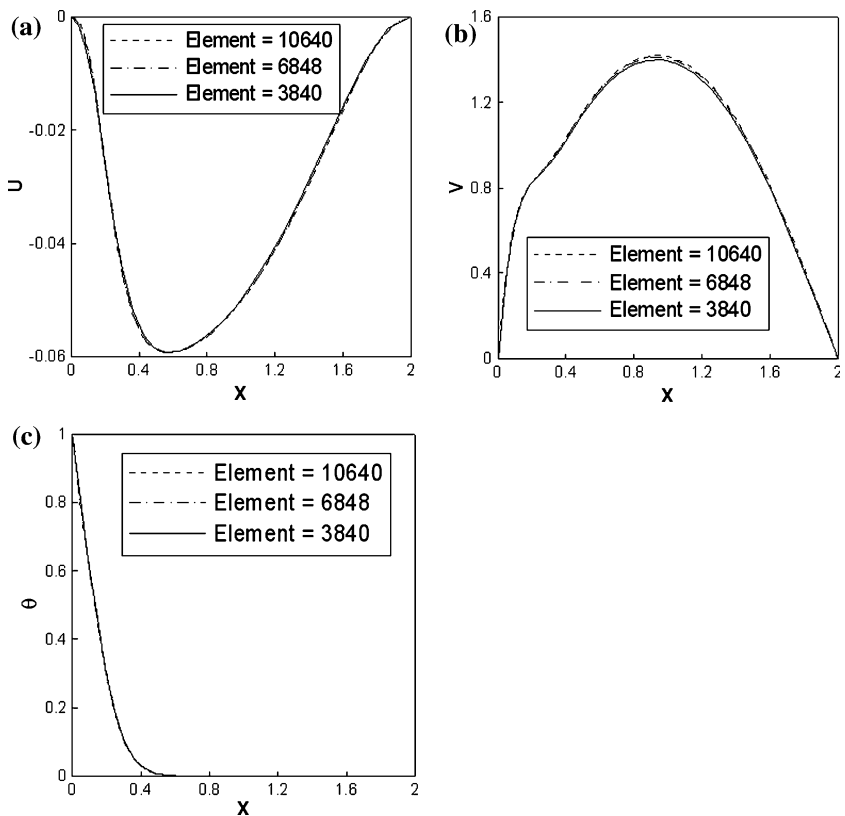


Fig. 3 Comparison of the variations of the average Nusselt numbers on the heat surface for different time step ($Gr = 10^4$, $Re = 10^2$, $L_c = 0.1$, $F_c = 2$)

$$\Delta\tau = \frac{1}{40 \times F_c} \quad (16)$$

At practical situations, the temperature difference between the IC under the operating situation simulated by the heat surface in this study and ambient air is usually smaller than

100°C, and the size of the IC's scale is close to 10⁻² m. Since this study includes both mixed convection and forced convections in laminar flow, the choice of the Reynolds number is 100 that is consistent with the ordination of Metais et al. [9] and Holman [5]. As for the Grashof number which is between 10⁰ and 10⁵.

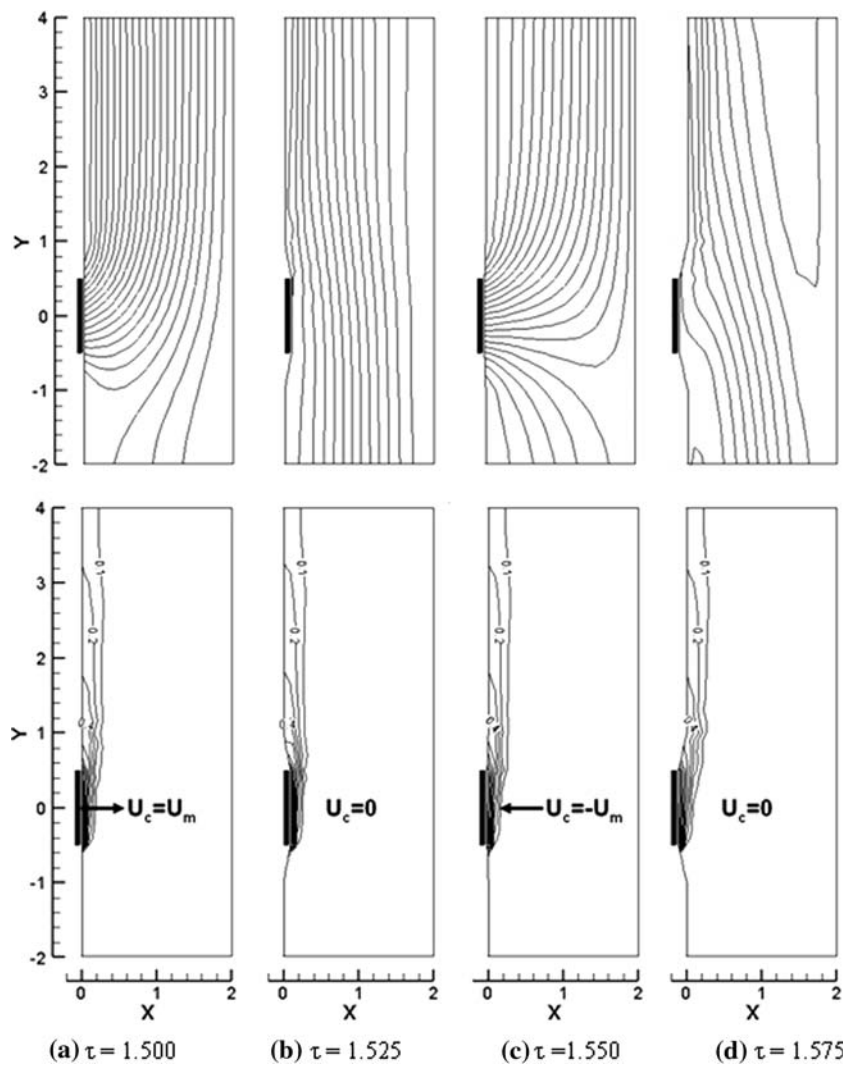
The dimensionless stream function Ψ is defined as

$$U = \frac{\partial\Psi}{\partial Y}, V = \frac{\partial\Psi}{\partial X} \quad (17)$$

For clearly indicating the variations of the flow and thermal fields, the streamlines and isothermal lines in the vicinity of the heat surface are presented only. Besides, the sign “arrow” in the subsequent figures is to indicate the moving direction of the heat surface.

For better understanding of the phenomena around the vibrational heat surface, the flow and thermal fields close to the vibrational heat surface are illustrated exclusively. Figure 4 indicates the variations of streamlines and isothermal lines under $Gr = 10^5$, $Re = 10^2$, $L_c = 0.1$, and $F_c = 10$ situation during the 16th periodic cycle in which the periodical variation occurs. Figure 4a is the initial stage of the 16th cycle or the final stage of the 15th cycle and $\tau = 1.5$. The position of the heat surface is at the center of the vibrational motion, the velocity of the heat surface moves toward the right and has the maximum speed. The

Fig. 4 The variations of the streamlines and isothermal lines during the 16th periodic cycle under $Gr = 10^5$, $Re = 10^2$, $L_c = 0.1$, and $F_c = 10$ situation



fluid near the heat surface is then extruded which causes the streamlines to be ejected from the heat surface and to flow upward due to the mixed convection effect. In Fig. 4b, the heat surface is at the right most side, the motion of the heat surface stops and the velocity equals to zero. Due to the convexity of the heat surface, the phenomena of ejection of the streamlines on the heat surface and neighboring regions can be slightly observed. But the above phenomena could be more apparent in the previous study by Fu and Huang [2] because of natural convection only. In Fig. 4c, the position of the heat surface is back to the center of the vibration motion, the velocity of the heat surface moves toward the left and has the maximum speed. The fluid is sucked by the heat surface, which leads the streamlines to flow toward the heat surface. In Fig. 4d, the heat surface is at the left most side and the speed of the heat surface is zero, the streamlines are still sucked to the left side but the trend becomes weak. As for the isothermal lines, the variations of the distribution of isothermal lines are close to

the heat surface, and the region of the isothermal lines distribution of the concave situation is slightly thicker than that of convex situation.

The variations of the time-average Nusselt numbers \overline{Nu} for per cycle with τ for $Gr = 10^3$, $Re = 10^2$ and $L_c = 0.1$ are shown in Fig. 5. When F_c is 30, the time-average Nusselt numbers are larger than that of the stationary state, and F_c is 20, the time-average Nusselt numbers decrease gradually and close to that of the stationary state finally. As $F_c = 10$, except the initial stage, the time-average Nusselt numbers are smaller than that of the stationary state.

Figure 6 indicates the variations of time-average Nusselt number \overline{Nu} for per cycle with time under $Gr = 10^4$, $Re = 10^2$ and $L_c = 0.1$ case. Since the mixed flow is aiding flow in this study, the Grashof number increases, the time-average Nusselt numbers are simultaneously to increase for each F_c situation. Similarly, the more the F_c is, the larger the \overline{Nu} could be obtained due to the drastic interaction between the vibrational heat surface and the flow.

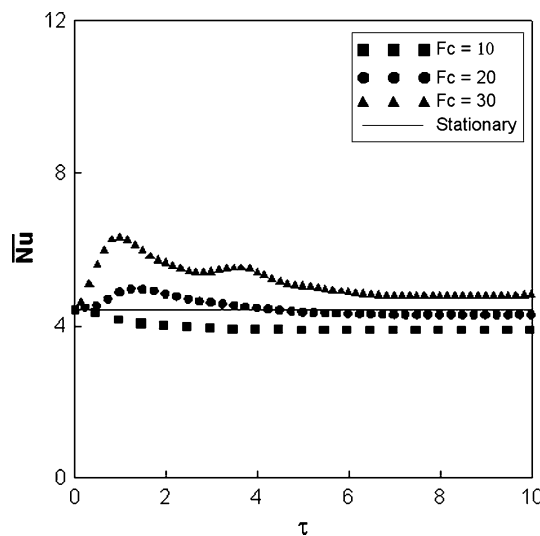


Fig. 5 The variations of the time-average Nusselt number \bar{Nu} for per cycle with time under $Gr = 10^3$, $Re = 10^2$ and $L_c = 0.1$

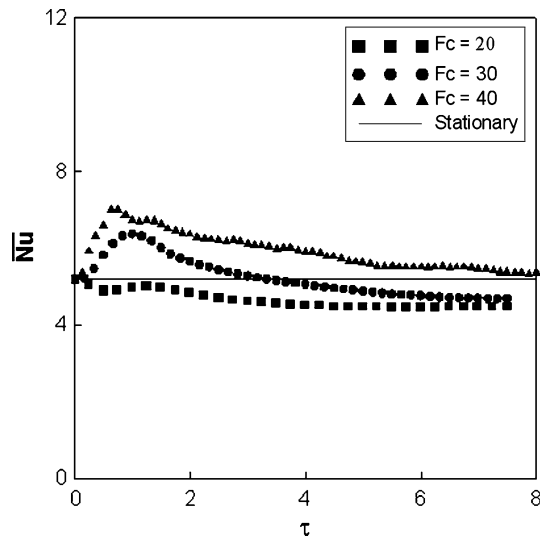


Fig. 6 The variations of the time-average Nusselt number \bar{Nu} for per cycle with time under $Gr = 10^4$, $Re = 10^2$ and $L_c = 0.1$

As the Grashof number increases to 10^5 , the variations of time-average Nusselt number \bar{Nu} for per cycle with time are shown in Fig. 7. As F_c exceeds about 70, the time-average Nusselt numbers begin to be larger than that of the stationary state. The high Grashof number situation means the natural convection to be drastic, the F_c of the vibration motion should then be larger in order to overcome the stronger natural convection.

Figure 8 shows the variations of the ratio of the time-average Nusselt number \bar{Nu} under the vibrational situation to the average Nusselt number Nu_{st} at the stationary state. The range of the vibration frequency is from 0.1 to 100. The corresponding frequency F_c of the ratio of the Nusselt

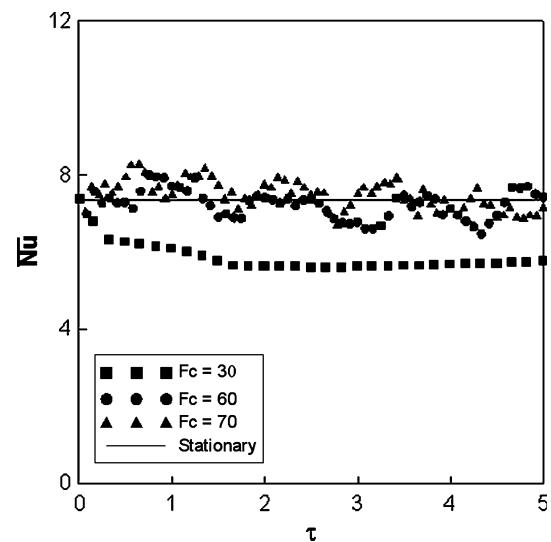


Fig. 7 The variations of the time-average Nusselt number \bar{Nu} for per cycle with time under $Gr = 10^5$, $Re = 10^2$ and $L_c = 0.1$

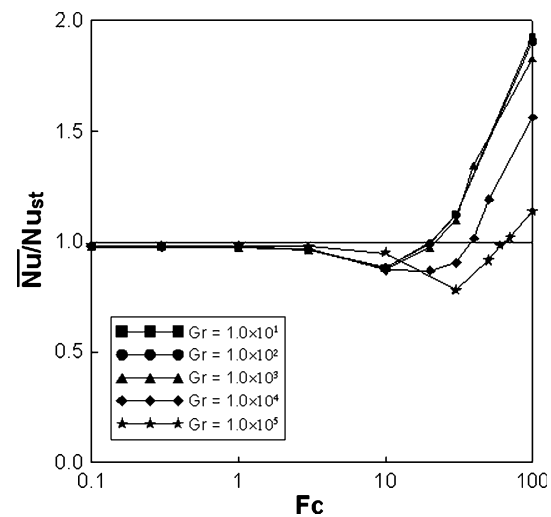


Fig. 8 The variations of the ratio of the time-average Nusselt number \bar{Nu} to the average Nusselt number Nu_{st} at the stationary state under $Re = 10^2$ and $L_c = 0.1$

numbers being more than 1.0 is between 10 and 100 under different Grashof numbers. As the ratio \bar{Nu}/Nu_{st} equals 1, the value of the frequency is defined as the critical vibration frequency F_{cc} proposed by Fu and Huang [2]. According to the definition, the vibrational frequency F_c is larger than the critical vibration frequency F_{cc} , the heat transfer is enhanced comparing with the stationary situation and vice versa.

Shown in Figs. 9 and 10, the variations of the ratio of the time-average Nusselt number \bar{Nu} under the vibrational situation to the average Nusselt number Nu_{st} at the stationary state for $L_c = 0.2$ and $L_c = 0.4$ are indicated, respectively. From these figures, the trend could be

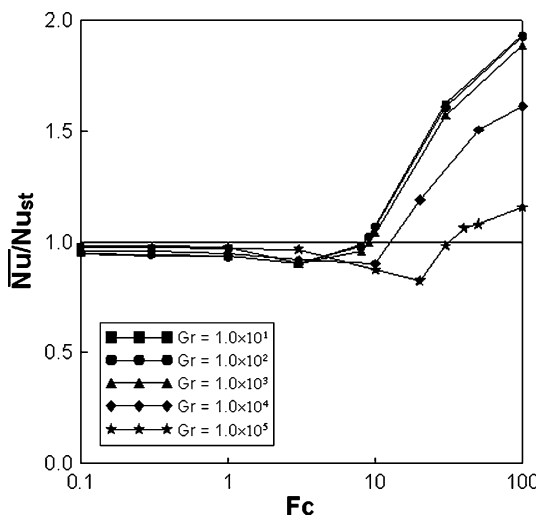


Fig. 9 The variations of the ratio of the time-average Nusselt number \bar{N}_u to the average Nusselt number $N_{u,st}$ at the stationary state under $Re = 10^2$ and $L_c = 0.2$

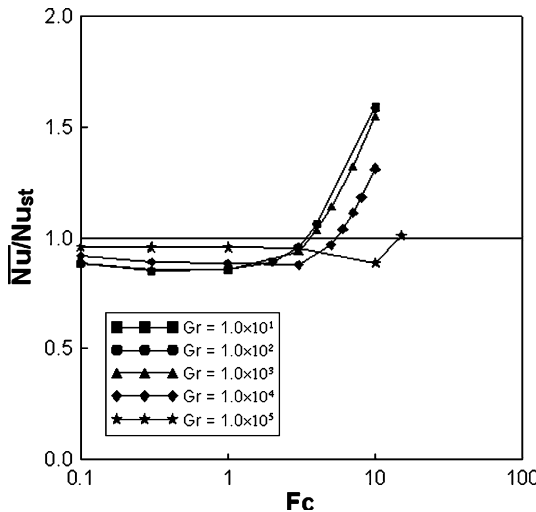


Fig. 10 The variations of the ratio of the time-average Nusselt number \bar{N}_u to the average Nusselt number $N_{u,st}$ at the stationary state under $Re = 10^2$ and $L_c = 0.4$

observed that the critical vibration frequency F_{cc} becomes smaller as the vibration amplitude L_c is larger. Since the larger amplitude causes the vibration velocity to be higher.

Generally, that a heat surface subject to a vibration motion is advantageous to convective heat transfer is a well-known tuition. However, based upon the results indicated above the heat transfer rates with certain combinations of the F_c and L_c are possibly smaller than that of the stationary condition. Then the critical vibration frequency F_{cc} could be regarded as a criterion of whether the heat transfer rate of the heat surface subject to a vibration motion being larger than that of the stationary state or not

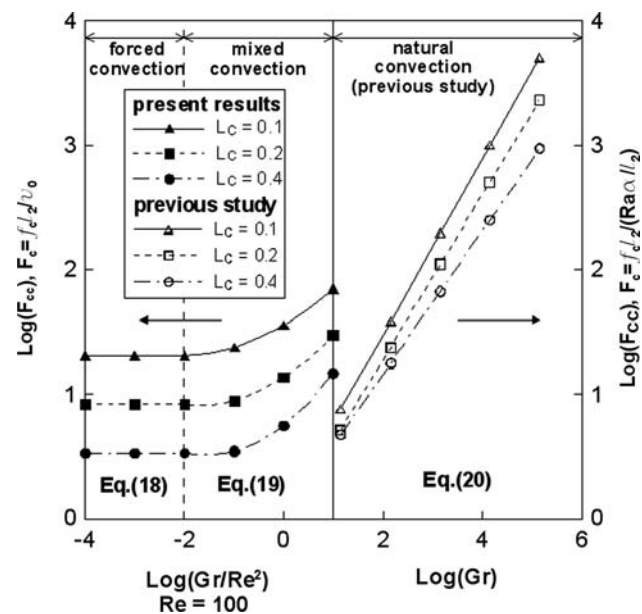


Fig. 11 The variations of the critical vibration frequency with Gr/Re^2 for forced and mixed convection and Gr for natural convection

and expressed as a function of Grashof number and vibration amplitude.

Usage of the results of Figs. 8, 9, and 10, the variations of the critical vibration frequency F_{cc} with Gr/Re^2 (for $Re = 10^2$) in different vibration amplitudes could be shown in Fig. 11 (solid symbols). The critical vibration frequency F_{cc} becomes smaller as the amplitude increases. However, as the Grashof number is smaller than 100, the critical vibration frequency F_{cc} is almost constant under a certain amplitude. The Reynolds number is limited mentioned earlier and equals 100, then the value of Gr/Re^2 is about 0.01 which is in the domain of a forced convection. Based upon the results, the critical vibration frequency F_{cc} of the forced convection being a constant under a certain amplitude could be obtained.

As the Gr/Re^2 is larger than 0.01, the increment of the critical vibration frequency F_{cc} varies monotonously with the augmentation of the Grashof number. Consequently, the phenomena mentioned above could be derived as the following Eqs. 18 and 19, respectively.

$$\log(F_{cc}) = 6.46L_c^2 - 5.85L_c + 1.83 \quad (\text{for } Re = 10^2) \quad (18)$$

$$\begin{aligned} \log(F_{cc}) = & (0.16L_c + 0.04) \log(Gr/Re^2)^2 \\ & + (0.27L_c + 0.21) \log(Gr/Re^2) \\ & + (7.53L_c^2 - 6.45L_c + 2.13), \quad (\text{for } Re = 10^2) \end{aligned} \quad (19)$$

The Eq. 18 expresses the forced convection domain and the Eq. 19 indicates the mixed convection domain.

The previous study investigated the effects of the vibrational heat surface on the natural convection exclusively. The equation in Fu and Huang [2] expressing the critical vibration frequency F_{cc} with a function of the amplitude and Rayleigh number could be rewritten as a function of the amplitude, and Grashof number and shown in the Eq. 20 (hollow symbols in Fig. 11) for leaguing with the present results (solid symbols in Fig. 11).

$$\begin{aligned} \log(F_{cc}) = & (-0.44L_c + 0.75) \log(Gr Pr) \\ & + (4.9L_c^2 - 2.7L_c + 0.4), \quad (\text{for } Pr = 0.71) \end{aligned} \quad (20)$$

Since Reynolds number is zero under a pure natural convection flow, two regions of mixed and natural convection flows should be divided to correlate the critical vibrational frequency. The parameters of Gr/Re^2 and Grashof number Gr are separately used in the mixed convection and natural convection regions as shown in Fig. 11. And the definitions of F_c are different in these two regions, $F_c = f_c \ell_2 / (\sqrt{Ra} \cdot \alpha / \ell_2)$ in the natural convection and $F_c = f_c \ell_2 / v_0$ in the mixed convection, respectively.

5 Conclusions

Effects of a vibrational heat surface on a mixed flow are investigated numerically. The variations of frequency, amplitude and Grashof number are considered and the results are examined in detail. The main conclusions could be summarized as follows.

1. The critical vibration frequency could be defined in terms of Grashof number and amplitude, and the frequency is larger than the critical vibration frequency which is advantageous to the heat transfer and vice versa.

2. In a forced convection, the critical vibration frequency is dependent on the amplitude only.
3. The equations of the critical vibration frequency expressing the variation from the forced convection via the mixed convection to the natural convection are separately derived, and vary smoothly through the above convection regions.

Acknowledgments The support of this work by Natural Science Council, Taiwan, ROC under contact NSC 93-2212-E-009-010 is gratefully acknowledged.

References

1. Andreozzi A, Bianco N, Naso V, Manca O (2005) Numerical analysis of opposing mixed convection in air in a vertical channel with a moving plate. *Proc ASME Heat Transf Div* 376:713–722
2. Fu WS, Huang CP (2006) Effects of a vibrational heat surface on natural convection in a vertical channel flow. *Int J Heat Mass Transf* 49:1340–1349
3. Fu WS, Yang SJ (2000) Numerical simulation of heat transfer induced by a body moving in the same direction as flowing fluids. *Heat Mass Transf* 36:257–264
4. Hirt CW, Amsden AA, Cooks HK (1974) An arbitrary Lagrangian–Eulerian computing method for all flow speeds. *J Comput Phys* 14:227–253
5. Holman JP (1992) Heat transfer, 7th edn. McGraw-Hill, New York
6. Kang BH, Jaluria Y (1990) Conjugate heat transfer from a continuously moving material in a parallel channel flow for cooling in forming manufacturing processes. *Proc ASME Heat Transf Div* 146:25–35
7. Kang BH, Jaluria Y (1994) Heat transfer from continuously moving material in channel flow for thermal processing. *J Thermophys Heat Transf* 8:546–554
8. Meric RA (1997) Simultaneous optimization of shape and flow parameters for combined free and forced convection in vertical channels. *Int J Numer Methods Eng* 40:551–563
9. Metais B, Eckert ERG (1964) Forced, mixed, and free convection regimes. *J Heat Transf Ser C* 86:295